Carbohydrate Polymers 94 (2013) 655–662

Contents lists available at SciVerse ScienceDirect

Carbohydrate Polymers

journal homepage: www.elsevier.com/locate/carbpol

Structure and properties of polypyrrole/bacterial cellulose nanocomposites

Daliana Muller[a,*], Carlos R. Rambo[b], Luismar. M. Porto[c], Wido H. Schreiner[d], Guilherme M.O. Barra[a,*]

[a] Department of Mechanical Engineering, Universidade Federal de Santa Catarina, Campus Universitário, CxP 476 Trindade, Florianópolis, SC 88040-900, Brazil
[b] Department of Electrical Engineering, Universidade Federal de Santa Catarina, Brazil
[c] Department of Chemical and Food Engineering, Universidade Federal de Santa Catarina, Brazil
[d] Departamento de Física da Universidade Federal do Paraná (UFPR), Curitiba, PR, Brazil

ARTICLE INFO

Article history:
Received 23 October 2012
Received in revised form 9 December 2012
Accepted 17 January 2013
Available online 4 February 2013

Keywords:
Polypyrrole
Bacterial cellulose
Ammonium persulfate
Iron III chloride hexahydrate

ABSTRACT

An electrically conducting composite based on bacterial cellulose (BC) and polypyrrole (PPy) was prepared through *in situ* oxidative polymerization of pyrrole (Py) in the presence of BC membrane using ammonium persulfate (APS), as an oxidant. The electrical conductivity, morphology, mechanical properties and thermal stability of the composites obtained using APS (BC/PPy·APS) were evaluated and compared with BC/PPy composites prepared using as oxidant agent Iron III chloride hexahydrate ($FeCl_3 \cdot 6H_2O$). The morphology of the BC/PPy·APS composites is characterized by spherical conducting nanoparticles uniformly distributed on the BC nanofiber surface, while the composites produced with $FeCl_3 \cdot 6H_2O$ (BC/PPy·$FeCl_3$) is composed of a continuous conducting polymer layer coating the BC-nanofibers. The electrical conductivity of BC/PPy·$FeCl_3$ was 100-fold higher than that found for BC/PPy·APS composites. In order to understand the site-specific interaction between PPy and BC functional groups, both composites were characterized by Fourier transform infrared (attenuated total reflectance mode) spectroscopy attenuation reflectance (FTIR-ATR) and X-ray photoelectron spectrometry (XPS). The affinity between functional groups of PPy·$FeCl_3$ and BC is higher than that found for BC/PPy·APS composite. In addition, the tensile properties were also influenced by the chemical affinity of both components in the polymer composites.

1. Introduction

Intrinsically conducting polymers (ICPs), such as polypyrrole (PPy) and polyaniline (PAni)-coated fibers with functional properties have been studied extensively due to their potential in many technological application, such as electronic displays (Spinks, Xi, Zhou, Troung, & Wallace, 2004), *scaffolds* for tissue engineering (Castro, Polo, Labrato, Cañete, & Rama, 2010; Cucchi et al., 2009; Stewart, Liu, Clark, Kapsa, & Wallace, 2012), smart sensors and actuators (Al-Mashat, Tran, Wlodarski, Kaner, & Kalantar-Zadeh, 2008; Savage, 2009), among others. A literature overview reveals interesting results concerning the use of fibers, such as polyester (Molina, Del Río, Bonastre, & Cases, 2009), polyamide (Kaynak, Najar, & Foitzik, 2008), cotton (Onar et al., 2009), cellulose derivate (Beneventi, 2010; Kelly, Johnston, Borrmann, & Richardson, 2007; Mo, Zhao, Chen, Niu, & Shi, 2009), and others, as a templates for preparing conducting polymer coated fibrous matrixes.

In recent years, considerable attention has been focused on the preparation of polypyrrole or polyaniline-coated nanofibers network through electrospinning technique, given the possibility to produce new nanostructured composites with the combination of high surface area, light weight, flexibility, toughness, high mechanical strength, fast diffusion of gas or liquid molecules, capacity to entrap biomolecules and serve as carriers in biological medium with the electrical, optical and magnetic behavior of ICPs (Chronakis, Grapenson, & Jakob, 2006; Ismail, Min, & Kim, 2009; Lee, Bashur, Goldstein, & Schmidt, 2009; Li, Guo, Wei, MacDiarmid, & Lelkes, 2006; Suttar et al., 2007). Despite the wide use of electrospinning for fabrication of conductive nanofibrous composites (Choi, Lee, Choi, Jung, & Shim, 2010), this process commonly involves organic solvent evaporation, which imparts a significant environmental impact. Among eco-friendly nanofibrous materials, bacterial cellulose (BC) has also been used as insulating polymer template to develop conductive polymer composites, especially because of its biocompatibility, low density, and noticeable properties of cellulose even in a hydrogel form (Rambo et al., 2008). BC can be mass produced in a wide variety of shapes and sizes through the control of cellulose biosynthesis in aqueous solution. In addition, this material exhibits interconnected nanofibers network similar to those prepared through electrospinning method.

There are some reports concerning the preparation of polyaniline-coated BC composites through *in situ* oxidative polymerization of aniline in BC membrane, using ammonium persulfate (APS) or Iron III chloride hexahydrate ($FeCl_3 \cdot 6H_2O$) (Hu, Chen, Yang, Liu, & Wang, 2011; Lee, Kim, & Yang, 2012a; Marins et al., 2011;

* Corresponding authors. Tel.: +55 48 3721 4019.
E-mail addresses: dalimuller@yahoo.com.br (D. Muller), guiga@emc.ufsc.br, G.Barra@ufsc.br (G.M.O. Barra).

0144-8617/$ – see front matter © 2013 Elsevier Ltd. All rights reserved.
http://dx.doi.org/10.1016/j.carbpol.2013.01.041

Müller et al., 2012). Lee et al. have recently published a report dealing the production of nanostructured conductive PAni/BC composites through interfacial polymerization (Lee, Chung, Kwon, Kim, & Tze, 2012b).

On the other hand, it has been reported previously by our research group the production of conducting composite composed of BC and polypyrrole (PPy) through *in situ* pyrrole (Py) polymerization on BC nanofibers, using $FeCl_3{\cdot}6H_2O$ (Müller, Rambo, Recouvreux, Porto, & Barra, 2011b). However, the correlation between structure and mechanical properties of BC/PPy·$FeCl_3$ system is particularly unclear. Moreover, it is well known that under aggressive reaction condition, such as high amount of $FeCl_3$ and strong acid medium, cellulose can be subjected to acid hydrolysis and degradation (Beneventi, Alila, Boufi, Chaussy, & Nortier, 2006). Through control of the polymerization conditions it is possible to produce PPy-coated fibers without a noticeable reduction in their mechanical properties when compared with those of pristine fibers (Dall'Acqua, Tonin, Peila, Ferrero, & Catellani, 2004; Dall'Acqua et al., 2006). Ferrero, Napoli, Tonin, and Varesano (2006) have studied the polymerization rate of Py on fibers surface using APS in the presence of different organic dopants in order to obtain PPy-coated fiber with suitable electrical conductivity and mechanical properties. In this context, the aim of this work is to obtain BC/PPy·APS composites with good electrical conductivity and mechanical properties through *in situ* oxidative polymerization of Py using APS without an organic dopant. The morphology, electrical conductivity, thermal and mechanical properties of BC/PPy·APS composites were evaluated and also compared with BC/PPy·$FeCl_3$ composites. The influence on site-specific interaction between PPy and BC functional groups of these resulting composites was also investigated.

2. Materials and methodology

Pyrrole (Merck, analytical grade) was distilled under vacuum and stored in refrigerator. Iron (III) chloride hexahydrate ($FeCl_3{\cdot}6H_2O$) (Vetec) and ammonium persulfate (APS) (Vetec) were used as received. The bacterial cellulose membranes were synthesized according to the procedure described in Rambo et al. (2008) by using the bacterial G. hansenii, ATC 558 232 strain in static culture conditions.

The polpypyrrole-coated bacterial cellulose composite (BC/PPy) was obtained through oxidative polymerization of pyrrole in

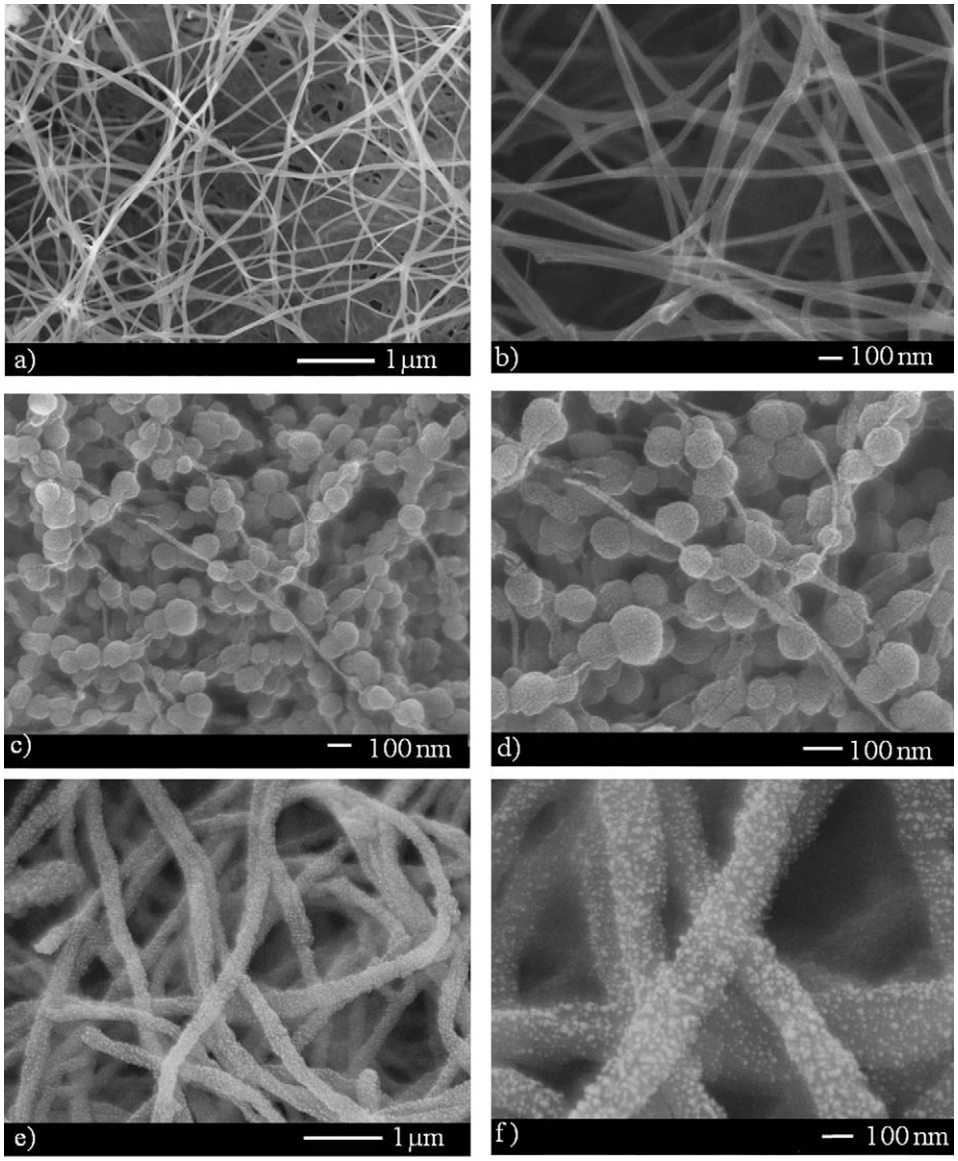

Fig. 1. FEG-SEM micrographs of (a and b) BC, (c and d) BC/APS and (e and f) BC/$FeCl_3$ samples.

hydrated BC membranes by following the method described in the literature (Müller et al., 2011b). In this procedure, hydrated BC membranes were immersed in pyrrole aqueous solution with concentration varying from 0.01 to 0.05 mol L^{-1}. In order to obtain BC/PPy composites with suitable electrical conductivity and mechanical properties, and prevent cellulose degradation, the APS/Py and $FeCl_3$/Py ratio used in this study was 0.18 and 1.3, respectively. The polymerization was carried out at room temperature by adding an aqueous solution of $FeCl_3$ or APS, as oxidant agents. After four hours, BC/PPy membranes were washed with distilled water and dried under vacuum at room temperature. BC/PPy samples prepared with APS or $FeCl_3$ are hereafter denoted as BC/PPy·APS and BC/PPy·$FeCl_3$, respectively.

3. Characterization

The morphology of the BC and composite surfaces was analyzed using a field-emission gun scanning electron microscopy (FEG-SEM, JEOL JSM-670F) operating at 15 kV and 80 A. Dried BC and PPy-coated BC membranes were placed over aluminum support and sputtered with gold.

Fourier Transform infrared (FTIR) spectra of pure BC, PPy and composites were obtained using a Bruker spectrometer (model Tensor 27) with an attenuated total reflectance accessory (ATR) in the range of 4000–700 cm^{-1} by accumulating 32 scans at a resolution of 4 cm^{-1}.

X-ray photoelectron spectrometry (XPS) measurements of the polymer samples were obtained using an ESCA3000 VG spectrometer with an MgK-α X-ray source (1253.6 eV) operating at 150 W. The electron analyzer was operated in an ultra high vacuum chamber, at approximately 10^{-9} mBar. To compensate for surface charging effects all binding energies were referenced to the C-1s neutral carbon peak (284.6 eV). Quantitative analysis of the XPS data was performed using the area ratio corrected by the sensitivity factor.

The amount of PPy deposited on BC membranes was determined by weighing dried BC samples (*Wi*) before and after pyrrole polymerization (*Wf*) at room temperature and relative humidity of 65%, as described in Eq. (1).

$$W\% = \frac{W_f - W_i}{W_f} \times 100 \quad (1)$$

Thermogravimetric analysis (TG) was used to determine the thermal stability of pure components and composites. TG was carried out with a STA 449 F1 Jupiter® (Netzsch) thermogravimetric analyzer. Non-isothermal experiments were carried out at 10 °C min^{-1} from 25 to 700 °C and Nitrogen flow was maintained constant at 50 cm^3 min^{-1}.

The electrical conductivity of the PPy and BC/PPy was determined using the four probe standard method with a Keithley 6220 current source and a Keithley Model 6517A electrometer.

Tensile strength tests of dried BC and BC/PPy composites with thicknesses in the range of 10–30 μm were performed using a dynamic mechanical analyzer (Q-800, TA Scientific) equipped with a clamp for films. The analysis was performed at room temperature and speed of 3 mm min^{-1}. The Young's modulus, tensile stress and elongation at break were determined from stress–strain curves, whereas at six analyses of each sample.

4. Results and discussion

Fig. 1 shows SEM-FEG micrographs of the pure BC and composites obtained through *in situ* method using APS or $FeCl_3$, as oxidants. The BC membrane is constituted by a network structure of interlaced cellulose nanofibers with high aspect ratio and mean diameter of 55 ± 20 nm. As shown in Fig. 1c and d, BC/PPy·APS composite is characterized by spherical PPy nanoparticles with a mean diameter of 90 ± 10 nm, which are uniformly distributed on BC nanofiber surfaces. On the other hand, BC/PPy·$FeCl_3$ composite is comprised of PPy nanoparticles with mean a diameter of 30 ± 20 nm that are fused together to form a continuous coating layer on BC nanofibers (core–shell like structure) (Müller et al., 2011b). The morphological differences between BC/PPy·APS and BC/PPy·$FeCl_3$ composites are probably related to the high affinity between BC and iron complexes formed during the Py polymerization in aqueous $FeCl_3$ solution. $FeCl_3$ hydrolysis leads to the formation of aquo-hydroxyl complexes and most of them are adsorbed on cellulose surfaces (Beneventi, Alila, Boufi, Chaussy, & Nortier, 2006; Kelly et al., 2007; Sasso et al., 2010). Under suitable reaction conditions, polymerization of pyrrole takes place preferentially on the cellulose fiber surface, forming a continuous conducting coating (Beneventi, 2010).

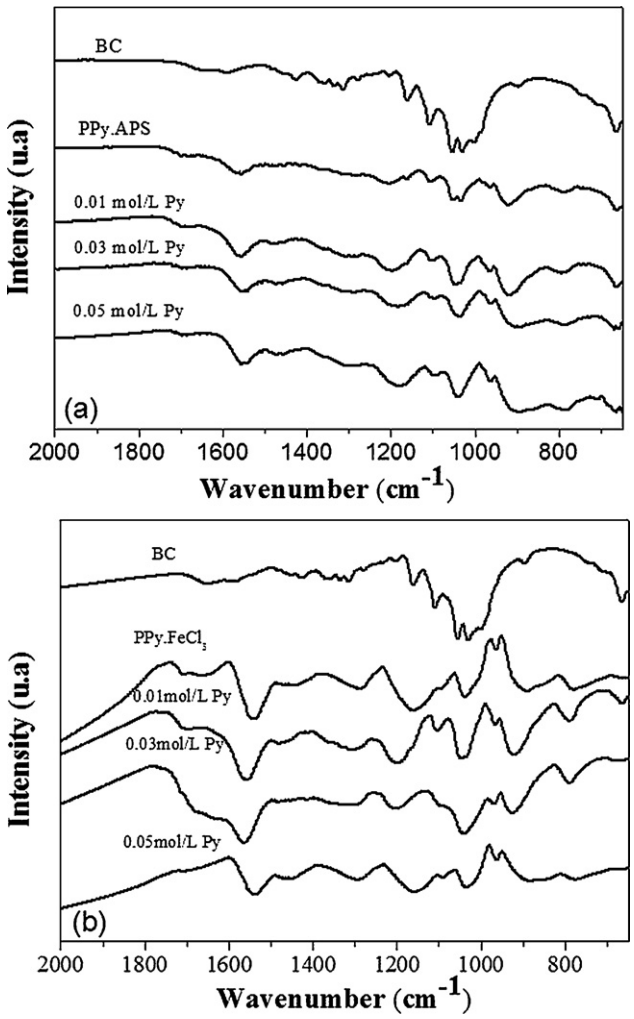

Fig. 2. FTIR spectra of (a) PPy·APS, BC, BC/PPy·APS composites and (b) PPy·$FeCl_3$, BC, BC/PPy·$FeCl_3$ composites.

FTIR spectra of PPy·APS, PPy·$FeCl_3$, BC and composites are shown in Fig. 2. The FTIR spectrum of BC showed broad absorption band in the region of 1060–1030 cm^{-1} assigned to C—O and C—O—C groups, which is in good agreement with the characteristic bands of BC reported in the literature (Rambo et al., 2008; Müller et al., 2011b). The typical spectral features of pure PPy prepared with both oxidants, APS and $FeCl_3$, are also observed in Fig. 2a and b. PPy·$FeCl_3$ sample exhibits two distinct bands at about 1535 and 1450 cm^{-1} which are attributed to C—C and C—N stretching vibrations in pyrrole ring, respectively. For pure PPy·APS, these absorption bands

Table 1
Elemental analysis, proportion of N species and doping degree of PPy·APS, PPy·$FeCl_3$ and composites obtained by XPS technique.

Samples	C (%)	N (%)	O (%)	S (%)	S/N	C/N	Proportion of			S/N–N^+	(%)
							=N—	—NH—	N^+		
BC/PPy·APS	43.0	10.2	43.7	3.1	0.3	4.2	0	0.82	0.18	0.12	18
PPy·APS	47.2	12.5	38.0	2.2	0.1	3.7	0	0.72	0.18	0	18
BC/PPy·$FeCl_3$	54.2	17.3	21.8	6.7	0.3	3.1	0.08	0.72	0.19	0.20	19
PPy·$FeCl_3$	64.8	16.2	15.6	3.4	0.2	4.0	0	0.80	0.20	~0	20

were blue-shifted to 1544 and 1460 cm^{-1}, probably due to the different doping degree of these two samples (Blinova, Stejskal, Trchová, Prokes, & Omastová, 2007). Moreover, the slight difference between PPy·APS and PPy·$FeCl_3$ spectra in the region of 1300–1100 cm^{-1} is attributed to the influence of the counter-ion group vibrations in the polymer backbone (Omastová, Trchová, Kovárová, & Stejskal, 2003).

FTIR spectra of composites exhibited overlapped absorption bands of both PPy and BC. The main difference in the spectra of BC/PPy·APS and BC/PPy·$FeCl_3$ composites was found in the region of 1545–1450 cm^{-1}. These bands were blue-shifted to 1551 and 1463 cm^{-1} for BC/PPy·$FeCl_3$ composites when compared with pure PPy·$FeCl_3$. This behavior suggests that vibrations involving the delocalized π electrons of PPy·$FeCl_3$ chains are affected by the presence of BC molecules due to the interactions between —N—H in the pyrrole ring and the —O—H groups of BC, as proposed by Johnston et al. (Johnston, Moraes, & Borrmann, 2005; Kelly et al., 2007. On the other hand, FTIR spectra of BC/PPy·APS composites are quite similar to that observed for pure PPy·APS, suggesting that in this system site-specific interaction of PPy·APS and BC functional groups is lower than that found for BC/PPy·$FeCl_3$.

The X-ray photoelectron spectrometry (XPS) has been shown to be a powerful tool for characterizing the surface composition and doping degree of intrinsically conducting polymer and their composites. The doping degree of PPy was determined by calculating the amount of different neutral and positively charged nitrogen of the PPy chain, as shown in Fig. 3. Both PPy·APS and PPy·$FeCl_3$ showed peaks with binding energies (BE) at 399.4 eV and 401 eV which are related to amine (—NH—) groups and the positively charged nitrogen (N^+), respectively, according to reports in the literature (Müller et al., 2011a; Joo et al., 2000). The BC/PPy·$FeCl_3$ composite exhibits an additional peak at 397.4 eV, corresponding to imine group (—N=), probably due to the presence of defects in the polymer backbone (Babu, Dhandapani, Maruthamuthu, & Kulandainathan, 2012). The proportion of the positively charged nitrogen of PPy in the BC/PPy·APS and BC/PPy·$FeCl_3$ composites is similar to that found for pure PPy, indicating that the doping degree of PPy was not affected by the presence of BC molecules.

Table 1 shows the elemental composition of pure components, proportion of N species and doping degree of PPy·APS, PPy·$FeCl_3$ and composites obtained by XPS technique. In general, doped PPy

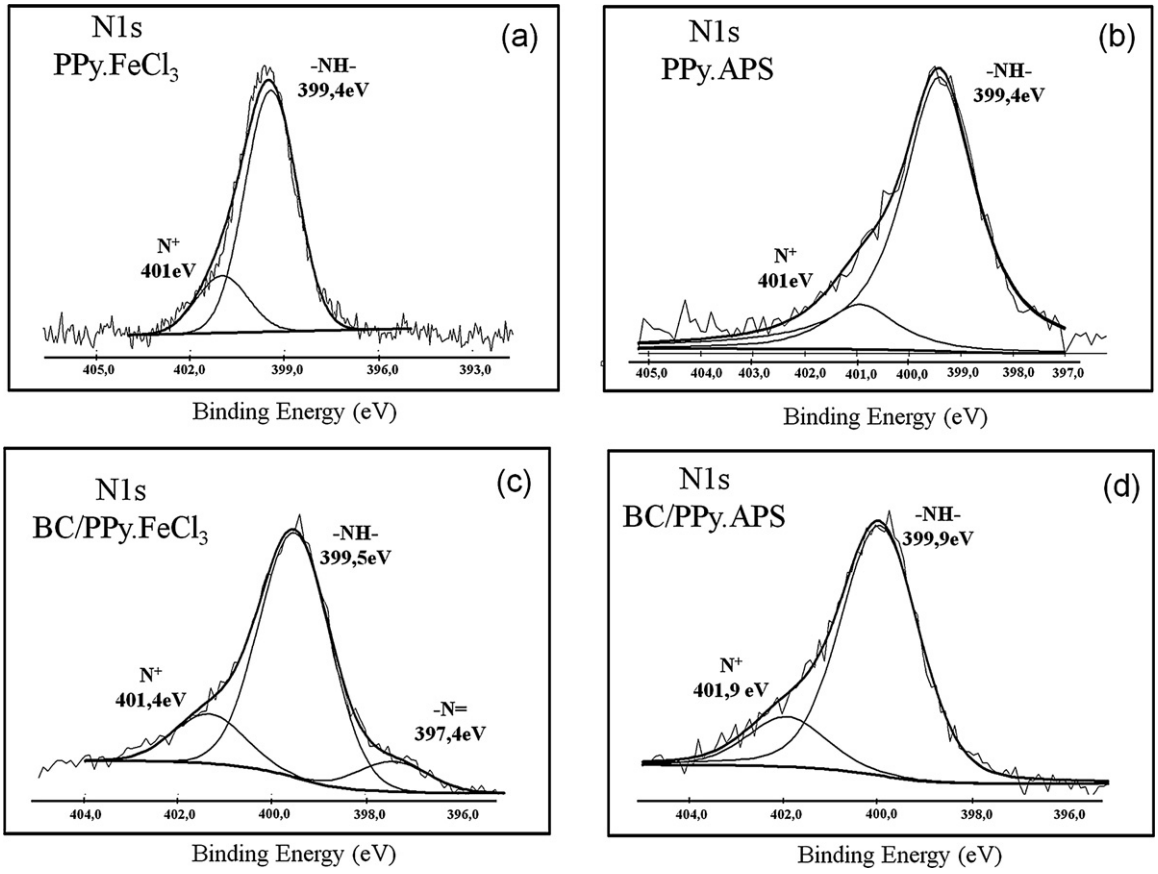

Fig. 3. Nitrogen 1s (N-1s) XPS core-level spectrum of (a) PPy·APS, (b) PPy·$FeCl_3$ and composites of (c) BC/PPy·APS and (d) BC/PPy·$FeCl_3$.

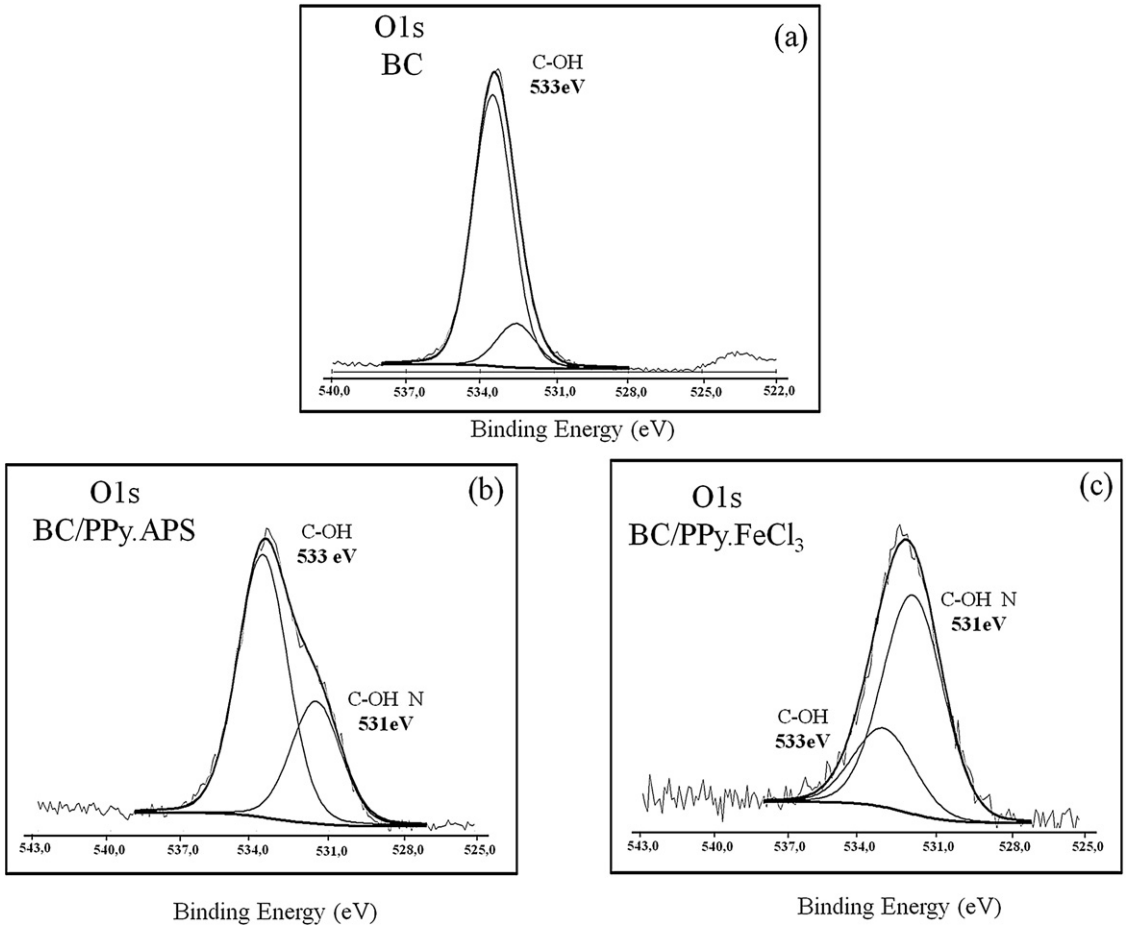

Fig. 4. Oxygen 1s (O-1s) XPS core-level stectrum of (a) BC, (b) BC/PPy·APS and (c) BC/PPy·$FeCl_3$.

contains theoretical C/N and S/N or Cl/N ratios of around 4.0 and 0.25, respectively. In this case, there is one positive charge per four pyrrole repeat units along the PPy backbone, which corresponds to a doping level of 25%. The molar ratio of PPy·APS and PPy·Cl_3 was lower than the theoretical values, which indicates that the doping degree of PPy obtained in this work is lower than 25%. However, BC/PPy composites present higher S/N or Cl/N molar ratio values than those found for pure PPy, suggesting that the doping degree of PPy deposited on BC fibers was higher than of pure PPy. This behavior can be confirmed by the percentage of nitrogen species in pure PPy and composites, which was determined from the properly curve-fitted N-1s core-level spectrum of composites and pure components (Fig. 3). For PPy·APS and PPy·$FeCl_3$ samples, the proportion of positively charged nitrogen (N^+) was about 0.20, which implies that the polymer chains contains one N^+ for every five pyrrole units. Even though PPy samples have the same doping degree, the electrical conductivity of PPy·$FeCl_3$ was 3.2 S cm^{-1} which was approximately 100-fold higher than that found for PPy·APS (1.3×10^{-2} S cm^{-1}). According Joo et al., the electrical conductivity of conducting polymers may be varied not only by the doping degree, but also due to the counter ion mobility and number of defects in the polymer chains (Joo et al., 2000). The amount of oxidant residues present as molecular species can be calculated from the difference between the S/N or Cl/N molar ratio and the proportion of positively charged nitrogen (S/N–N^+), as shown in Table 1. Note that BC/PPy·APS and BC/PPy$FeCl_3$ composites showed a significant difference between S/N and Cl/N molar ratio and the positively charged nitrogen. Although these samples had been washed several times with distilled water in order to remove the excess of the byproducts and residues of the reaction, this result indicates the presence of oxidant residues in both composites.

Table 2
Parameters of thermal analysis (TG), PPy content determined by gravimetric analysis and electrical conductivity of pure components and composites.

Samples	Py content (mol L^{-1})	Onset temp. (°C)	Residue (%)	PPy content[a] (%)	Electrical conductivity (S cm^{-1})
BC	–	285	22.0 ± 1.5	–	1.8×10^{-13}
PPy·APS	–	218	56.7 ± 1.4	–	1.3×10^{-2}
PPy·$FeCl_3$	–	175	60.7 ± 1.7	–	3.2×10^{0}
BC/PPy·APS	0.01	265	25.9 ± 2.8	12.0 ± 2.0	7.8×10^{-7}
BC/PPy·APS	0.03	265	29.6 ± 2.1	23.3 ± 1.5	2.5×10^{-5}
CB/PPy·APS	0.05	265	32.5 ± 2.9	33.1 ± 2.5	1.2×10^{-2}
BC/PPy·$FeCl_3$	0.01	240	46.6 ± 3.4	49.6 ± 3.3	3.7×10^{-3}
BC/PPy·$FeCl_3$	0.03	230	57.8 ± 3.6	73.3 ± 2.5	1.1×10^{-1}
BC/PPy·$FeCl_3$	0.05	230	60.2 ± 3.9	80.0 ± 2.0	2.7×10^{0}

[a] Gravimetric analysis.

Table 3
Tensile properties of BC, BC/PPy·APS and BC/PPy·$FeCl_3$ composites prepared with 0.01, 0.03 and 0.05 pyrrole concetration in the polymerization medium.

Py concentration (Mol L^{-1})	BC/PPy·APS			BC/PPy·$FeCl_3$		
	σ (MPa)	ε (%)	E (GPa)	σ (MPa)	ε (%)	E (GPa)
0	60.1 ± 3.8	2.0 ± 0.2	5.1 ± 0.3	60.1 ± 3.8	2.0 ± 0.2	5.1 ± 0.3
0.01	55.5 ± 4.6	1.8 ± 0.3	3.2 ± 0.5	24.7 ± 4.1	7.8 ± 0.7	0.3 ± 0.06
0.03	28.8 ± 4.9	2.3 ± 0.5	1.3 ± 0.4	8.2 ± 1.2	4.2 ± 0.4	0.2 ± 0.08
0.05	18.5 ± 5.4	4.8 ± 0.7	0.5 ± 0.6	4.1 ± 1.7	3.5 ± 0.9	0.1 ± 0.05

Fig. 4 shows oxygen XPS spectra for the BC, BC/PPy·APS and BC/PPy·$FeCl_3$ composites. The BC membrane exhibits peaks with binding energy (BE) at 533.4 eV and 532.6 eV which is related to hydroxyl (—OH) and ether (—C—O—C—) groups, respectively (Pertile, Andrade, Alves, & Gama, 2010). The main peak at 533 eV becomes less pronounced when compared with BC/PPy·APS and BC/PPy·$FeCl_3$ composites. This observation corroborates the suggestion made by Kelly et al. and Beneventi et al., previously discussed in FTIR analyses, that site-specific interaction between the —N—H and —O—H functional groups is operative in both composites (Beneventi, Alila, Boufi, Chaussy, & Nortier, 2006; Kelly et al., 2007). These data also revealed that there are considerable fractions of bonded hydroxyl-amine group even in BC/PPy·APS composites, as illustrated in Fig. 4b. Furthermore, a more pronounced decrease in the proportion of —OH group was observed for BC/PPy·$FeCl_3$ composite (Fig. 4c), probably due to the higher site-specific interaction of functional groups than those found for BC/PPy·APS composite.

TG curves of BC, PPy·APS, PPy·$FeCl_3$ and composites are shown in Fig. 5. PPy samples showed a small weight loss below 100 °C related to the release of water and low-molecular weight pyrrole oligomers. The weight loss between 180 and 300 °C was attributed to the counter ions and the loss above 400 °C corresponds to the thermal degradation of the main chain (Nyström et al., 2010). TG curve of BC exhibited two distinct decomposition steps. The first corresponds to the water loss, while the second was attributed to the decomposition of cellulose backbone (Rambo et al., 2008). TG curves of both BC/PPy composites prepared with different monomer content reveal that there were two weight loss steps related to the water elimination and thermal degradation of both components.

The main degradation parameters, PPy content estimated by gravimetric analysis (GA) and electrical conductivity of pure BC and composites are illustrated in Table 2. The composites residues, the amount of PPy deposited on BC nanofibers and the electrical conductivity increased with increasing monomer concentration. The composites showed lower onset degradation temperature than that of pure BC, due to the loss of intermolecular hydrogen bonds of cellulose by the presence of conducting polymer (Marins et al., 2011; Lee et al., 2012a; Müller et al., 2012). On the other hand, the PPy deposited on the nanofiber surface starts to decompose at higher temperature when compared with pure PPy·APS and PPy·$FeCl_3$ samples, *i.e.*, the onset degradation temperature of PPy·APS and PPy·$FeCl_3$ shifts from 218 °C to 265 °C and 175 °C to 230 °C for BC/PPy·APS and BC/PPy·$FeCl_3$ composites, respectively. This behavior can be attributed to the site-specific interaction between PPy and cellulose groups. As expected, the degradation temperature change is more pronounced for BC/PPy·$FeCl_3$ composites due to the higher site specific interactions between BC and PPy than those found for BC/PPy·APS composites, as it was previously mentioned in XPS and FTIR analysis. Furthermore, in the PPy·$FeCl_3$-coated system the electrical conductivity is higher than that found for BC/PPy·APS composite. This behavior can be explained by three main reasons: (i) the highest electrical conductivity of PPy·$FeCl_3$ coating layer; (ii) BC/PPy·$FeCl_3$ composite showed higher PPy content than those found for BC/PPy·APS system at the same monomer concentration; and finally, (iii) morphological differences between BC/PPy·$FeCl_3$ and BC/PPy·APS composites, as previously discussed in MEV-FEG micrographs.

The tensile properties of BC, BC/PPy·APS and BC/PPy·$FeCl_3$ composites are shown in Table 3. BC membrane showed typical brittle behavior with elongation at break lower than 2.0 ± 0.2%. The tensile strength and Young's Modulus of pure BC are approximately 65 ± 3.7 MPa and 5.1 ± 0.3 GPa, respectively. The tensile properties results of pure BC and composites showed significant dispersion due to their morphology which is comprised of a network structure of randomly interlaced cellulose nanofibers. In both composites, the tensile strength and Young's modulus decreased with increasing Py content, which is a result of the reduction of the hydrogen bonding

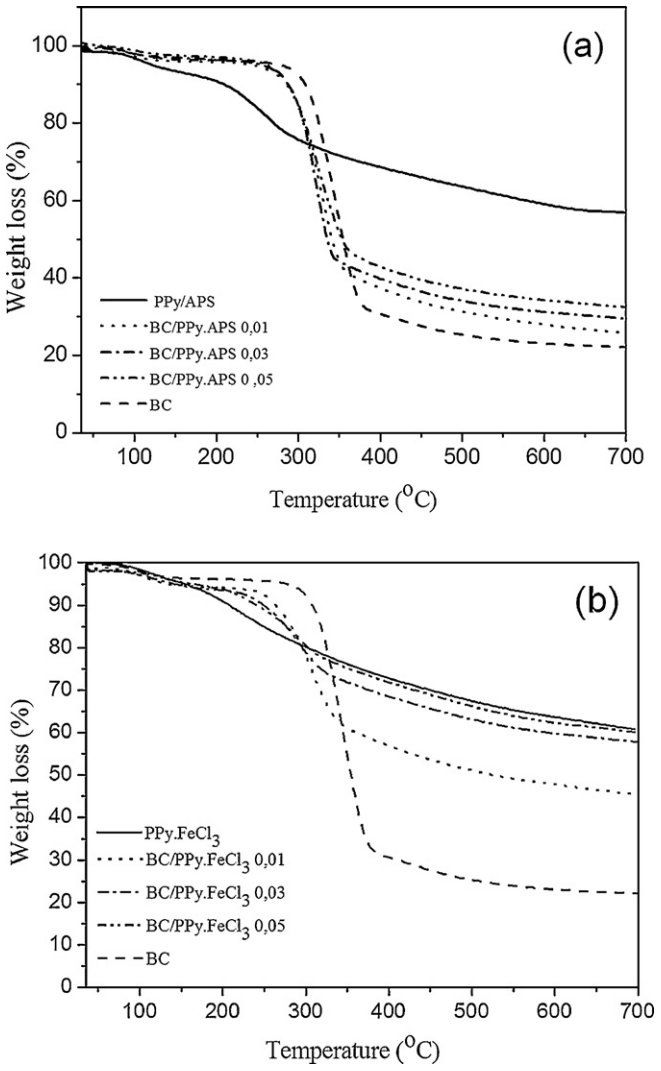

Fig. 5. TG curves of pure (a) PPy·APS, BC BC/PPy·APS and (b) PPy·$FeCl_3$, BC, BC/PPy·$FeCl_3$.

of BC due to the presence of PPy particles adhered on nanofibers surfaces. The elongation at break of BC/PPy·APS composites enhanced with increasing the amount of PPy particles deposited on BC nanofibers due to the same reason discussed previously. On the other hand, for composites prepared with Py concentrations of 0.01 Mol L^{-1}, the elongation at break initially increases, but tends to decrease with increasing of PPy·$FeCl_3$ content on nanofibers surface. Important to note that the tensile properties of BC/PPy·APS composites are higher than those found for BC/PPy·$FeCl_3$. This behavior can be also attributed to the higher cellulose degradation, characterized by a significant reduction of the hydrogen bonding of cellulose molecules when compared with the BC/PPy·APS composites.

5. Conclusion

Flexible and conducting BC/PPy·APS composites with electrical conductivity in the range of 0.01–1.2 S cm^{-1} and good mechanical properties (40 MPa) were prepared through *in situ* oxidative chemical polymerization of pyrrole (PPy) in the presence of BC hydrogel using APS or $FeCl_3 \cdot 6H_2O$, as an oxidant agent. FEG-SEM analysis revealed that pyrrole polymerized with BC membranes using APS is characterized by PPy nanoparticles with a mean diameter of 90 ± 10 nm distributed uniformly on BC nanofibers. On the other hand, BC/PPy·$FeCl_3$ composites prepared with $FeCl_3$ exhibited a core–shell-like structure. The FTIR and XPS analysis showed that site-interaction between —NH and —OH groups of PPy and BC components, respectively, was operative in both composites. However, BC/PPy·$FeCl_3$ composite presented higher interaction of functional groups than BC/PPy·APS. Finally, this work showed that the type of oxidant and monomer concentration used in the oxidative chemical polymerization of pyrrole in a BC hydrogel is crucial to control the structure and properties of BC/PPy composites, and hence, their use in suitable technological applications.

Acknowledgments

The authors gratefully acknowledge the financial support of the Brazilian Council for Scientific and Technological Development (CNPq), Coordination for the Improvement of Higher Level Personnel (CAPES-Brazil), and Fundação de Amparo à Pesquisa e Inovação do Estado de Santa Catarina (FAPESC). The authors also thank the Central Electronic Microscopy Laboratory (LCME-UFSC) for the microscopy analysis.

References

Al-Mashat, L., Tran, H. D., Wlodarski, W., Kaner, R. B., & Kalantar-zadeh, K. (2008). Polypyrrole nanofiber surface acoustic wave gas sensors. *Sensors and Actuators B*, *134*, 826–831.

Babu, K. F., Dhandapani, P., Maruthamuthu, S., & Kulandainathan, M. A. (2012). One pot synthesis of polypyrrole silver nanocomposite on cotton fabrics for multifunctional property. *Carbohydrate Polymers*, *90*, 1557–1563.

Beneventi, D., Alila, S., Boufi, S., Chaussy, D., & Nortier, P. (2006). Polymerization of pyrrole on cellulose fibres using a $FeCl_3$ impregnation- pyrrole polymerization sequence. *Cellulose*, *13*, 725–734.

Beneventi, T.-L. S. (2010). Highly conducting polypyrrole/cellulose nanocomposite films with enhanced mechanical properties. *Macromolecular Materials and Engineering*, *295*, 932–941.

Blinova, N. V., Stjskal, J., Trchová, M., Prokes, J., & Omastová, M. (2007). Polyaniline and polypyrrole: A comparative study of the preparation. *European Polymer Journal*, *43*, 2331–2341.

Castro, J. E. C., Polo, J. L., Labrado, G. R. H., Cañete, V. P., & Rama, C. G. (2010). Bioelectrochemical control of neural cell development on conducting polymers. *Biomaterials*, *31*, 9244–9255.

Choi, J., Lee, J., Choi, J., Jung, D., & Shim, S. E. (2010). Electrospun PEDOT:PSS/PVP nanofibers as the chemiresistor in chemical vapour sensing. *Synthetic Metals*, *160*, 1415–1421.

Chronakis, I. S., Grapenson, S., & Jakob, A. (2006). Conductive polypyrrole nanofibers via electrospinning: Electrical and morphological properties. *Polymer*, *47*, 1597–1603.

Cucchi, I., Bosch, A., Arosiob, C., Bertini, F., Freddi, G., & Catellani, M. (2009). Bio-based conductive composites: Preparation and properties of polypyrrole (PPy)-coated silk fabrics. *Synthetic Metals*, *159*, 246–253.

Dall'Acqua, L., Tonin, C., Varesano, A., Canetti, M., Porzio, W., & Catellani, M. (2006). Vapour phase polymerization of pyrrole on cellulose-based textile substrates. *Synthetic Metals*, *156*, 379–386.

Dall'Acqua, L., Tonin, C., Peila, R., Ferrero, F., & Catellani, M. (2004). Performances and properties of intrinsic conductive cellulose-polypyrrole textile. *Synthetic Metals*, *146*, 213–221.

Ferrero, F., Napoli, L., Tonin, C., & Varesano, A. (2006). Pyrrole chemical polymerization on textiles: Kinetics and operating conditions. *Journal of Applied Polymer Science*, *102*, 4121–4126.

Hu, W. L., Chen, S., Yang, Z., Liu, L., & Wang, H. (2011). Flexible electrically conductive nanocomposite membrane based on bacterial cellulose and polyaniline. *Journal of Physical Chemistry B*, *26*, 8453–8457.

Ismail, Y. A., Min, K. S., & Kim, S. J. (2009). A nanofibrous hydrogel templated elecrochemical: From single mat to a rolled-up structrure. *Sensors and Actuators B: Chemical*, *136*, 438–443.

Johnston, J. H., Moraes, J., & Borrmann, T. (2005). Conducting polymers on paper fibres. *Synthetic Metals*, *153*, 65–68.

Joo, J., Lee, S. Y., Lee, J. K., Jang, S. K., Oh, E. J., & Epstein, A. J. (2000). Physical characterization of electrochemically and chemically. *Macromolecules*, *33*, 5131–5136.

Kaynak, A., Najar, S. S., & Foitzik, R. C. (2008). Conducting nylon, cotton and wool yarns by continuous vapor polymerization of pyrrole. *Synthetic Metals*, *158*, 1–5.

Kelly, F. M., Johnston, J. H., Borrmann, T., & Richardson, M. J. (2007). Functionalized hybrid materials of conducting polymers with individual fibres of cellulose. *European Journal of Inorganic Chemistry*, *35*, 5571–5577.

Lee, B. H., Kim, H.-J., & Yang, H.-S. (2012). Polymerization of aniline on bacterial cellulose and characterization of bacterial cellulose/polyaniline nanocomposite films. *Journal of Current Applied Physics*, *12*, 75–80.

Lee, H.-J., Chung, T.-J., Kwon, H.-J., Kim, H.-J., & Tze, W. T. Y. (2012). Fabrication and evaluation of bacterial cellulose-polyaniline composites by interfacial polymerization. *Cellulose*, *19*, 1251–1258.

Lee, Y. j., Bashur, C. A., Goldstein, A. S., & Schmidt, C. E. (2009). Polypyrrole-coated electrospun PLGA nanofibers for neural tissue applications. *Biomaterials*, *30*, 4325–4335.

Li, M., Guo, Y., Wei, Y., MacDiarmid, A. G., & Lelkes, P. I. (2006). Electrospinning polyaniline-contained gelatin nanofibers for tissue engineering applications. *Biomaterials*, *27*, 2705–2715.

Marins, J. A., Soares, B. G., Dahmouche, K., Ribeiro, S. J. L., Barud, H., & Bonemer, D. (2011). Structure and properties of conducting bacterial cellulose-polyaniline nanocomposites. *Cellulose*, *18*, 1285–1294.

Mo, Z.-l., Zhao, Z.-l., Chen, H., Niu, G.-p, & Shi, H.-f. (2009). Heterogeneous preparation of cellulose-polyaniline conductive composites with cellulose activated by acids and its electrical properties. *Carbohydrate Polymers*, *75*, 660–664.

Molina, J., Del Río, A. I., Bonastre, J., & Cases, F. (2009). Electrochemical polymerisation of aniline on conducting textiles of polyester covered with polypyrrole/AQSA. *European Polymer Journal*, *45*, 1302–1315.

Müller, D., Garcia, M., Salmoria, G. V., Pires, A. T. N., Paniago, R., & Barra, G. M. O. (2011a). SEBS/PPy·DBSA blends: Preparation and evaluation of electromechanical and dynamic mechanical properties. *Journal of Applied Polymer Science*, *120*, 351–359.

Müller, D., Mandelli, J. S., Marins, J. A., Soares, B. G., Porto, L. M., Rambo, C. R., et al. (2012). Electrically conducting nanocomposites: preparation and properties of polyaniline (PAni)-coated bacterial cellulose nanofibers (BC). *Cellulose*, *19*, 1645–1654.

Müller, D., Rambo, C. R., Recouvreux, D. O. S., Porto, L. M., & Barra, G. M. O. (2011b). Chemical *in situ* polymerization of polypyrrole on bacterial cellulose nanofibers. *Synthetic Metals*, *161*, 106–111.

Nyström, G., Mihranyan, A., Razaq, A., Lindström, T., Nyholm, L., & Strømme, M. (2010). A nanocellulose polypyrrole composite based on microfibrillated cellulose from wood. *Journal Physical of Chemistry B*, *114*, 4178–4182.

Omastová, M., Trchová, T., Kovárová, J., & Stejskal, J. (2003). Syntesis and structural study of polypyrroles prepared in the presence of surfactants. *Synthetic Metals*, *138*, 447–455.

Onar, N., Akşit, A. C., Ebeoglugil, M. F., Birlik, I., Celik, E., & Ozdemir, I. (2009). Structural, electrical, and electromagnetic properties of cotton fabrics coated with polyaniline and polypyrrole. *Journal of Applied Polymer Science*, *114*, 2003–2010.

Pertile, R. A. N., Andrade, F. K., Alves, C., Jr., & Gama, M. (2010). Surface modification of bacterial cellulose by nitrogen-containing plasma for improved interaction with cells. *Carbohydrate Polymers*, *82*, 692–698.

Rambo, C. R., Recouvreux, D. O. S., Carminatti, C. A., Pitlovanciv, A. K., Antônio, R. V., & Porto, L. M. (2008). Template assisted synthesis of porous nanofibrous cellulose membranes for tissue engineering. *Materials Science and Engineering C*, *28*, 549–554.

Sasso, C., Zeno, E., Petit-Coni, M., Chaussy, D., Belgacem, M. N., & Beneventi, T.-L. S. (2010). Highly conducting polypyrrole/cellulose nanocomposite films with

enhanced mechanical properties. *Macromolecular Materials and Engineering*, *295*, 932–941.
Savage, N. O. (2009). Gas sensing composites of metal oxides with vapor-deposited polypyrrole. *Sensors and Actuators B*, *143*, 6–11.
Spinks, G. M., Xi, B., Zhou, D., Truong, V. T., & Wallace, G. G. (2004). Enhanced control and stability of polypyrrole electromechanical actuators. *Synthetic Metals*, *140*, 273–280.
Stewart, E. M., Liu, X., Clark, G. M., Kapsa, R. M. I., & Wallace, G. G. (2012). Inhibition of smooth muscle cell adhesion and proliferation on heparin-doped polypyrrole. *Acta Biomaterialia*, *8*, 194–200.
Suttar, D. S., Padma, N., Aswal, D. K., Deshpande, S. K., Gupta, S. K., & Yakhmo, J. V. (2007). Preparation of nanofibrous polyaniline films and their application as ammonia gas sensor. *Sensors and Actuators B: Chemical*, *128*, 286–292.